



A comparison of data weighting methods to derive vertical land motion trends from GNSS and altimetry at tide gauge stations

Marcel Kleinherenbrink¹, Riccardo Riva¹, and Thomas Frederikse¹

¹Department of Geoscience and Remote Sensing, Delft University of Technology, P.O. Box 5048, 2600 GA Delft, The Netherlands

Correspondence to: Marcel Kleinherenbrink (m.kleinherenbrink@tudelft.nl)

Abstract. This study compares eight weighting techniques for Global Navigation Satellite System (GNSS)-derived Vertical Land Motion (VLM) trends at 570 tide gauge (TG) stations. The spread between the methods has a comparable size as the formal uncertainties of the GNSS trends. Taking the median of the surrounding GNSS trends shows the best agreement with differenced altimetry - tide gauge (ALT-TG) trends. An attempt is also made to improve VLM trends from ALT-TG time series. Only using highly correlated along-track altimetry and TG time series, reduces the standard deviation of ALT-TG time series up to 10%. As a result, there are spatially coherent changes in the trends, but the reduction in the RMS of differences between ALT-TG and GNSS trends is insignificant. However, setting correlation thresholds also acts like a filter to remove problematic TG stations. This results in sets of ALT-TG VLM trends at 344-663 TG locations, depending on the correlation threshold. Compared to other studies, we decrease the RMS of differences between GNSS and ALT-TG trends (from 1.47 to 1.22 mm yr⁻¹), while we increase the number of locations (from 109 to 155). Depending on the weighting methods the mean of differences between ALT-TG and GNSS trends varies between 0.1-0.2 mm yr⁻¹. We reduce the mean of differences by taking into account the effect of elastic deformation due to present-day mass redistribution into account.

1 Introduction

Tide Gauges (TGs) measure local relative sea level, which means that they are affected by geocentric sea level, but also by Vertical Land Motion (VLM). Knowing VLM at TGs is essential to convert the observed sea level into a geocentric reference frame, in which among others satellite altimeters operate. TGs used in sea level reconstructions also require a correction for VLM. The mean of VLM at TGs is not equal to that of the basin, and therefore local VLM estimates are required to get an accurate estimate of ocean volume change. Several VLM processes are modelled. On a global scale the largest VLM trend in TG records is Glacial Isostatic Adjustment (GIA), which typically reaches values of 10 mm yr⁻¹ in Canada and Scandinavia (Ostanciaux *et al.*, 2012). On large scales present-day mass redistribution also affects the trends and due to the accelerating rate of Greenland's ice mass loss, and to a lesser extent other processes, it accelerates them. Trends at TGs are also affected by a large number of other local signals, including erosion, ground water depletion, postseismic deformation and gas extraction (Hamlington *et al.*, 2016; Wöppelmann and Marcos, 2016). Since the local VLM processes cannot be captured by models, and the large-scale processes contain large uncertainties, observations of VLM at TGs are essential.



One method to estimate VLM at TGs uses geodetic Global Positioning System (GPS) receivers at fixed stations or Doppler Orbitography and Radiopositioning Integrated by satellite (DORIS) observations. Since many other navigation satellites are currently providing range estimates as well, we will refer to the GPS stations as Global Navigation Satellite System (GNSS) stations. Most studies compute GNSS VLM at TG stations from one of the datasets by University of La Rochelle (ULR) (Wöppelmann *et al.*, 2007; Pfeffer and Allemand, 2016; Wöppelmann *et al.*, 2014; Wöppelmann and Marcos, 2016). Even though ULR contains several GNSS solution inland, its main focus is the coastal zone. Currently, 754 GNSS stations are processed in the ULR6 database. A more extensive database with approximately 14000 GNSS is processed by the Nevada Geodetic Laboratory (NGL). They use a different processing procedure to estimate trends from time series, which makes trends less vulnerable to jumps (Blewitt *et al.*, 2016). A statistical comparison between several GNSS solutions was recently made by Santamaría-Gómez *et al.* (2017). They concluded that the number of stations in the NGL database was larger, but that the accuracy was on average significantly lower than the ULR6 stations. They also discussed systematic errors due to differences in the origin of the reference frames, which were in the order of 0.2 mm yr^{-1} globally. Furthermore, they found that the local VLM uncertainty at tide gauge was increased by $4 \times 10^{-3} \text{ mm yr}^{-1}$ per kilometer distance between the TG and the GNSS station (Santamaría-Gómez *et al.*, 2017). Most studies use the trends of either co-located GNSS stations or the closest GNSS station or the mean of all GNSS stations within a radius of several tens of kilometers (Santamaría-Gómez *et al.*, 2014; Pfeffer and Allemand, 2016). Only Hamlington *et al.* (2016) involved a more complex GNSS weighting procedure using NGL trends, based on a combination of spatial filtering, Delaunay triangulation and median weighting. One way to quantify the accuracy of GNSS-based VLM trends at TGs is to compute the spread of individual geocentric sea level estimates or the spread of geocentric sea level between regions (Wöppelmann and Marcos, 2016). The spread of regional trends reduced from 0.9 mm yr^{-1} in the ULR1 solution (Wöppelmann *et al.*, 2007) to 0.5 mm yr^{-1} in the ULR5 solution (Wöppelmann *et al.*, 2014), which is approximately the expected residual climatic signal. Any further improvements in the GNSS trends require therefore another validation technique.

A second way to observe VLM at TGs, to overcome the limitations of sparsely distributed GNSS network, is differencing satellite altimetry and TG time series, which we will refer to as ALT-TG time series from here on. Initially, the ALT-TG time series were used to monitor the stability of satellite altimeters for the Global Mean Sea Level (GMSL) record, which is currently guaranteed up to 0.4 mm yr^{-1} (Mitchum, 1998, 2000). The first study to infer VLM trends from ALT-TG time series was Cazenave *et al.* (1999). Based on the method of Mitchum (1998) they compared ALT-TG to DORIS at six stations. Later, several studies were conducted on regional and global scale of which an overview is given by Ostanciaux *et al.* (2012). The first study to estimate more than 100 VLM trends (Nerem and Mitchum, 2002) obtained error bars for 60 of 114 TGs smaller than 2 mm yr^{-1} . However, they noted that the TGs should be inspected on a case-by-case basis to determine if the result was truly VLM. Ostanciaux *et al.* (2012) increased the number of ALT-TG VLM trend estimates sixfold to 641, but it included some outliers with trends above 20 mm yr^{-1} . They also made a comparison between their study and several earlier studies. The best agreement was found over a small set of 28 tide gauges, where the results of Ostanciaux *et al.* (2012) differed from (Ray *et al.*, 2010) by an RMS of 1.2 mm yr^{-1} .



Recently, several studies have compared the GNSS trends to those of ALT-TG globally (*Santamaría-Gómez et al.*, 2014; *Wöppelmann and Marcos*, 2016; *Pfeffer and Allemand*, 2016). Several other studies did an equivalent comparison with DORIS and ALT-TG for a limited number of stations (*Cazenave et al.*, 1999; *Nerem and Mitchum*, 2002; *Ray et al.*, 2010). While the older studies primarily used along-track data from the Jason (TOPEX/POSEIDON (TP), Jason-1 (J1) and Jason-2 (J2)) series of satellite altimeters, the latest studies used preprocessed grids and *Wöppelmann and Marcos* (2016) made a comparison between several gridded products and one along-track dataset. All recent studies used ULR5 GNSS trends for comparison. The best results were obtained with an interpolated altimetry grid provided by AVISO (*Pujol et al.*, 2016), yielding a median of differences of 0.25 mm yr^{-1} with an RMS of 1.47 mm yr^{-1} based on a comparison at 107 locations (*Wöppelmann and Marcos*, 2016). It is important to note that the time series for all sites were visually inspected, primarily to remove those with non-linear behaviour. Additionally, the corresponding correlation between altimetry and TG time series were found to be highest for AVISO. *Pfeffer and Allemand* (2016) did not apply visual inspection and obtained a comparable result for 113 stations (an RMS of 1.7 mm yr^{-1}), while only incorporating GNSS trends from stations within 10 km from the tide gauge.

This study aims to further reduce the discrepancies between GNSS and ALT-TG trends, while increasing the number of trend pairs. To do this, we will apply several steps to improve the VLM estimates at tide gauges. First of all, the number of reliable trend estimates are increased by using the GNSS trends from the larger NGL database. Most TGs will neighbour multiple GNSS stations for which several weighting methods are applied to determine the best procedure. Correlations between altimetry and TG time series are exploited to reduce residual ocean variability, which is often present in ALT-TG time series (*Vinogradov and Ponte*, 2011). The reduction in ocean variability should lead to more reliable ALT-TG VLM trends. Correlation thresholds additionally function as a filter, to remove time series that are uncorrelated due to differences in ocean signals and possible (undocumented) jumps in the TG time series. Additionally, we address the problem of contemporary mass redistribution on trends over different time spans using a fingerprinting method.

2 Data and Methods

In this section, we describe the processing procedures for deriving direct and differenced VLM trends for comparison at TG locations. First, we will address the estimation of GNSS trends at the TG locations. The estimation of ALT-TG differenced trends is discussed in several steps. We briefly discuss the selection of the tide gauges. After that we will discuss the altimetry processing procedures. We briefly review the Hector software (*Bos et al.*, 2013) for the estimation of trends from differenced ALT-TG time series. Eventually, trend corrections for contemporary mass redistribution using fingerprinting methods are described.

2.1 GNSS trends

The trend estimation at tide gauges primarily deals with two problems. First, a trend has to be estimated from a GNSS time series, which contains an autocorrelated noise signal, and often undocumented jumps. This is discussed in Sect. 2.1.1. Second, since many GNSS stations are not directly co-located to the tide-gauge station, the assumption is made that both are affected



by the same VLM signal. When multiple GNSS receivers are present in the vicinity of the tide gauge, a weighting method is required to estimate a single VLM trend. This is discussed in Sect. 2.1.2.

2.1.1 Trend estimation

To obtain VLM trends at TGs, often the products of the Université de La Rochelle (ULR) are used. ULR version 6 makes use of the Create and Analyze Time Series (CATS) software (Williams, 2008), which is able to estimate trends and errors from time series, taking into account temporally correlated noise. Next to a slight change in trend, it has the advantage that it computes a more realistic trend uncertainty. However, the frequently occurring jumps, due to earthquakes or equipment changes, decrease the accuracy, which is therefore often larger than 1 mm yr^{-1} (Gazeaux *et al.*, 2013).

In this study the results of NGL (Blewitt *et al.*, 2016) are used. Blewitt *et al.* (2016) proposed the Median Interannual Difference Adjusted for Skewness (MIDAS) approach, which is based on the Theil-Sen estimator. The procedure estimates trends from couples of daily data points separated by 365 days. It then removes all measurements outside two standard deviations, computed by scaling the median of absolute deviations, with respect to the median of the trend couples. Afterwards, a new median is computed, which serves as the trend estimate. Blewitt *et al.* (2016) demonstrated that MIDAS has a smaller equivalent step detection size than methods which included step detection, as those used by ULR. Besides the advantage of detecting smaller jumps, approximately 14000 GNSS time series are processed, which is almost 20 times more than ULR6.

2.1.2 Station weighting and selection

Despite several recommendations to co-locate GNSS receivers with TGs, only a few have a record long enough to estimate reliable trends. Therefore we take all stations into account that are within 50 km from a TG, provided that the standard deviation on the trend is lower than 1 mm yr^{-1} as estimated from the MIDAS algorithm. Most studies simply average all neighbouring TG trends or take the trend from the closest station. However, many other and possibly better, techniques are possible. We compare trends from several approaches in Sect. 3.1 and with the ALT-TG trends in Sect. 3.3.

In total eight different approaches are considered. The first two involve all of the trends neighbouring GNSS stations by computing their mean [1] and median [2]. Method [1] is among others applied by (Frederikse *et al.*, 2016) for regional sea level reconstructions. One of the most frequently applied approach uses the trend at the closest station [3]. It is used in two recent studies by Santamaría-Gómez *et al.* (2012) and Pfeffer and Allemand (2016). We also investigate inverse distance weighting [4] in which the trend $\frac{dh_{TG}}{dt}$ is estimated as:

$$\frac{dh_{TG}}{dt} = \frac{\sum \frac{1}{d_i} \frac{dh_i}{dt}}{\sum \frac{1}{d_i}}, \quad (1)$$

where d_i and $\frac{dh_i}{dt}$ represent the distance to the tide gauge station and the trend at GNSS station i . We also use the GNSS trends based on the longest time series [5] and smallest error [6]. The seventh approach involves weighting with the variances σ_i^2 of



the trends [7], such that:

$$\frac{dh_{TG}}{dt} = \frac{\sum \frac{1}{\sigma_i^2} \frac{dh_i}{dt}}{\sum \frac{1}{\sigma_i^2}}. \quad (2)$$

And the last method [8] takes into account spatial dependency and trend uncertainty by combining methods [4] and [7], i.e. by weighting with the variance and with the distance. Method [8] is a variant to the technique used in the altimeter calibration study of *Watson et al.* (2015). Note that in several studies the weighting method for GNSS trends is not documented.

2.2 Tide gauge time series

Monthly TG data are obtained from the PSMSL database (*Holgate et al.*, 2012). All time series flagged after 1993 are removed. Any observations that are outside of 1 meter from the mean are considered outliers and removed from the data. This number is similar to our altimetry sea level threshold and based on the criterion used by NOAA for their global mean sea level estimates (*Masters et al.*, 2012). To be consistent with the altimetry observations, we apply a Dynamic Atmosphere Correction (DAC) consisting of a low-frequency inverse barometer correction and short-term wind and pressure effects *Carrère and Lyard* (2003). Initially, we consider all TGs with at least 10 years of valid data.

2.3 Differenced ALT-TG time series

Wöppelmann and Marcos (2016) obtained the smallest standard deviation in the differenced time series by averaging grid cells within 1 degree from the TG using the AVISO interpolated product. The results obtained by taking the most correlated grid point from AVISO within 4 degrees around the TG increased the standard deviation. *Wöppelmann and Marcos* (2016) obtained lower correlations by averaging Goddard Space Flight Center (GSFC) along-track altimetry measurements within a radius of 1 degree from the TG. Note that the AVISO grid is constructed using correlation radii of 50-300 km (*Ducet et al.*, 2000) and it includes measurements from all altimetry satellites, not only the Jason series. The AVISO grid therefore effectively averages over a much larger radius around the TG and it includes observation from more satellites. The larger uncorrelated noise using GSFC compared to AVISO, as shown by the combination of the increased RMS and the spectral index (*Wöppelmann and Marcos*, 2016), is therefore likely an effect of the limited number of GSFC altimetry measurements. However, using the large effective radius of AVISO might increase the correlated noise, due to the inclusion sea level observations far away from the TG, which do not correlate with the sea level observed at the tide gauge. This can result in a remaining ocean signal in ALT-TG time series, which contaminates the VLM trend estimates.

To overcome the limitations of gridded products, we work with along-track data and exploit the correlations between sea level at the satellite measurement location and at the TG on interannual and decadal scales by using a low-pass filter. We start by creating sea level time series every 6.2 km along-track using the measurements from TP, J1 and J2 from the RADS database (*Scharroo et al.*, 2012) between 1993-2015. In order to get a consistent set of altimetry observations, the same geophysical correction are used for all satellites, which are given in Table 1. All time series within 250 km from the TG are taken into account.



Table 1. List of geophysical corrections and orbits applied in this study.

Satellite	T/P	Jason-1&2
Orbits	CCI	GDR-E
Ionosphere	Smoothed dual-frequency	
Wet troposphere	Radiometer	
Dry troposphere	ECMWF	
Ocean tide	GOT4.10	
Loading tide	GOT4.10	
Solid Earth tide	Cartwright	
Sea state bias	CLS	
Mean sea surface	DTU15	
Dynamic atmosphere	MOG2D	

Additionally, intermission biases between TP-J1 and J1-J2 are removed. *Ablain et al.* (2015) revealed a large dependence of the intermission biases on the latitude. For the J1-J2 differences, a single polynomial is estimated through the differences between the sea level observations of both instrument, such that the correction $\Delta h_{sla,ib}(\lambda)$ becomes:

$$\Delta h_{sla,ib}(\lambda) = c_0 + c_1 \cdot \lambda + c_2 \cdot \lambda^2 + c_3 \cdot \lambda^3 + c_4 \cdot \lambda^4, \quad (3)$$

5 with λ the latitude of the altimetry observations. For the TP-J1 differences, separate polynomials are estimated for four latitude regions and the ascending/descending tracks (*Ablain et al.*, 2015). The values for the parameters c_n are given in Table 2.

The Jason satellite series samples sea level every ten days, hence we average monthly 3-4 measurements in order to make a first set of time series that is compatible with the monthly TG observations. As for the case of the TG monthly solutions, observations more than 1 m from the mean sea surface are removed and the time series should have at least 10 years of valid
 10 observations. Additionally, a second set of monthly time series at each satellite measurement location is created, by applying a yearly moving-average filter. This second set of altimetry time series is correlated with a low-pass filtered version of the TG series, in order to test whether their signals match on interannual and longer time scales. The yearly moving-average filter allows to suppress the noise present in individual altimetry measurements. The full pole tide from RADS is subtracted from both time series before correlation, whereas for the TG time series we restore the solid Earth pole tide as computed in *Desai et al.* (2015). We also remove residual seasonal cycles and a linear trend before correlation. An iterative procedure removes sea
 15 surface heights outside of 3 RMS up to a maximum of 10 % of the observations. The outlier removal is primarily implemented to remove any spurious data present in the RADS database. It is unlikely that more than 10 % of the observations contain processing problems or outliers due to extreme events. If more observations would be discarded, high correlations might not represent corresponding ocean signal anymore. The result is a set of correlations that indicate which altimetry sea level time
 20 series resemble the TG time series on interannual time scales and longer.



Table 2. Values for the parameters of the latitudinal intermission bias correction. These numbers are added to the sea surface height anomalies of the respective satellites.

Parameter	TP asc.		TP desc.		Jason-2	
	Lat(deg)	Value	Lat(deg)	Value	Lat(deg)	Value
c_0 (mm)	(-66.2,-1.5)	80.3	(-66.2,-1.5)	77.3	(-66.2,66.2)	98.1
c_1 (mm deg ⁻¹)		$-2.3 \cdot 10^{-1}$		$-1.7 \cdot 10^{-1}$		$-9.3 \cdot 10^{-2}$
c_2 (mm deg ⁻²)		$-1.1 \cdot 10^{-2}$		$1.2 \cdot 10^{-3}$		$3.8 \cdot 10^{-3}$
c_3 (mm deg ⁻³)		$-3.0 \cdot 10^{-4}$		$2.9 \cdot 10^{-4}$		$8.4 \cdot 10^{-7}$
c_4 (mm deg ⁻⁴)		$-2.4 \cdot 10^{-6}$		$3.8 \cdot 10^{-6}$		$7.6 \cdot 10^{-7}$
c_0 (mm)	(-1.5,0.2)	83.8	(-1.5,1.3)	79.9		
c_1 (mm deg ⁻¹)		1.3		2.4		
c_2 (mm deg ⁻²)		-1.3		$5.2 \cdot 10^{-1}$		
c_3 (mm deg ⁻³)		$-5.3 \cdot 10^{-1}$				
c_4 (mm deg ⁻⁴)						
c_0 (mm)	(0.2,4)	84.9	(1.3,4)	73.3		
c_1 (mm deg ⁻¹)		$-8.0 \cdot 10^{-1}$		13.7		
c_2 (mm deg ⁻²)		$-8.6 \cdot 10^{-1}$		-5.1		
c_3 (mm deg ⁻³)		$1.5 \cdot 10^{-1}$		$4.9 \cdot 10^{-1}$		
c_4 (mm deg ⁻⁴)						
c_0 (mm)	(4,66.2)	72.9	(4,66.2)	75.8		
c_1 (mm deg ⁻¹)		$8.1 \cdot 10^{-1}$		$7.9 \cdot 10^{-1}$		
c_2 (mm deg ⁻²)		$-2.8 \cdot 10^{-2}$		$-3.3 \cdot 10^{-2}$		
c_3 (mm deg ⁻³)		$3.4 \cdot 10^{-4}$		$6.4 \cdot 10^{-4}$		
c_4 (mm deg ⁻⁴)		$-1.1 \cdot 10^{-6}$		$3.9 \cdot 10^{-6}$		

The monthly low-pass filtered altimetry time series are kept, if the corresponding correlation are above a certain threshold. We combine the remaining altimetry time series, to get one averaged altimetry time series per TG. Alternatively, we also use the correlations as weights, to get one correlation-weighted altimetry time series per tide gauge. In this case the monthly low-pass filtered time series are weighted by their corresponding correlation, then added together and accordingly normalized, so that the weights sum up to one. The resulting time series are subtracted from the TG time series if there are at least ten altimetry time series with a correlation above the threshold. The resulting differenced ALT-TG time series with less than 15 years of valid observations are further discarded. This last requirement is due to the fact that remaining ocean signals can still affect the estimated trends significantly. An example of the reduction of variability due to correlation thresholds and weighting is shown in Fig. 1. The white noise in the unfiltered time series is reduced in the red curve, however the opposite might happen if the number of altimetry time series decreases. Most important is to note that there is a strong reduction in the variance of temporally correlated residuals, represented here by the low-pass filtered time series. Correlated residual signal can strongly



affect the estimated trend, especially in areas with large interannual variability due to interannual event like ENSO. Note that for the differentiation of the time series only the solid Earth part of the pole tide is added to the TGs, but this time as is done in the IERS2010 conventions (*Petit and Luzum, 2010*), such that the trends are consistent with those of the GNSS data. The main difference is that the altimetry pole tide correction of *Desai et al. (2015)* are computed with respect to linearly drifting mean pole, while in the IERS conventions the mean pole location is modelled as a third order polynomial. If the pole tide is not taken into account consistently, it can introduce biases of 0.1 mm yr^{-1} (*Santamaría-Gómez et al., 2017*). Since the change rate of the mean pole is non-linear, this will introduce trend biases if the time spans between GNSS and altimetry do not match. This is corrected for using the mass redistribution fingerprints discussed in Sect. 2.5.

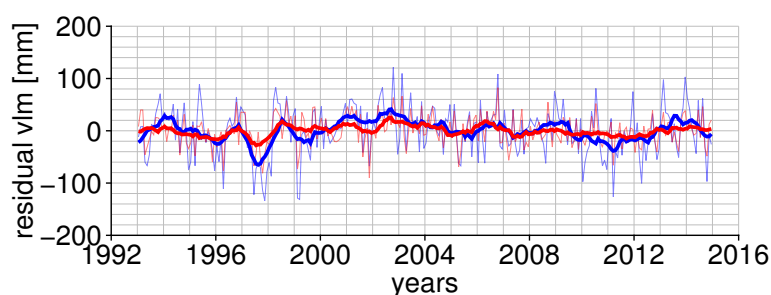


Figure 1. Low-pass filtered time series of ALT-TG differenced VLM at Winter Harbour. In blue: without a threshold on the correlation. In red: with a threshold of 0.7 for the correlation and with correlation weighting. In the background the time series without a low-pass filter applied.

2.4 Differenced ALT-TG trends

For the computation of the trends and the corresponding standard deviation, we fit a power-law in combination with a white noise model by using the Hector software (*Bos et al., 2013*). The spectrum of the white noise is flat, while the spectrum of power-law noise, $P(f)$, decays with frequency and is given by (*Bos et al., 2013*):

$$P(f) = \frac{1}{f_s^2} \frac{\sigma^2}{(2 \sin(\pi f / f_s))^{2d}}, \quad (4)$$

where f_s is the sampling frequency, σ the power-law noise scaling factor and d links to the spectral index κ in *Wöppelmann and Marcos (2016)* by $\kappa = -2d$. The value of d affects the effective number of autoregressive parameters (*Bos et al., 2013*). This is required to capture the temporal correlation in the ALT-TG time series as shown by Fig. 2 in which the low-pass filtered time series give an idea of the memory in the system. In order to handle several weakly non-stationary ALT-TG time series we use the function 'PowerlawApprox', which uses a Toeplitz approximation for power-law noise (*Bos et al., 2013*).

2.5 Contemporary mass redistribution

The trends estimated from GNSS time series are computed over different time spans than the ALT-TG trends and will be affected by non-linear VLM induced by elastic deformation due to present-day ice melt and changes in land hydrology stor-

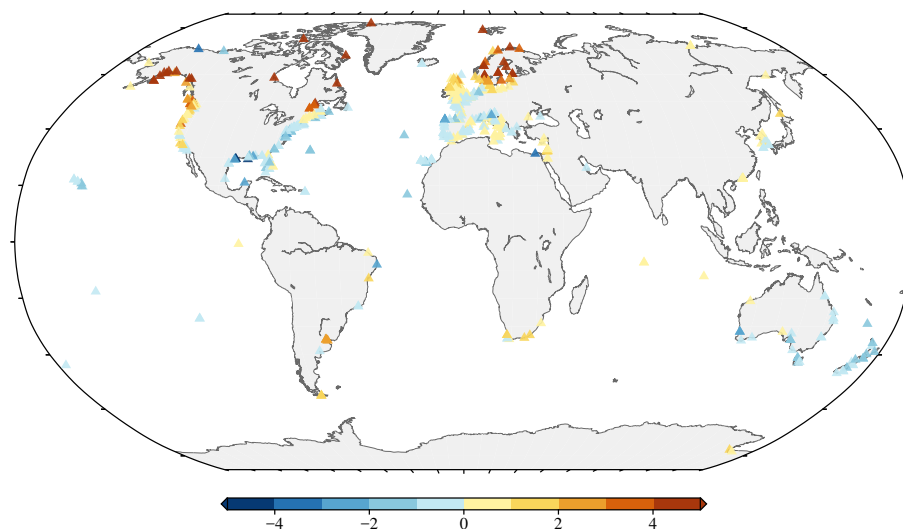


Figure 2. VLM (mm/yr) at TGs using the median of the neighbouring trends.

age (Riva *et al.*, 2017). To quantify those non-linear VLM signals, the response to mass redistribution is computed using a fingerprinting method at yearly resolution. We take into account the loads of Greenland, Antarctica and glacier mass loss, the effects of dam retention and hydrological loads. A detailed description of the input loads is given in (Frederikse *et al.*, 2016). To estimate the fingerprints of VLM, the sea level equation is solved, including the rotational feedback (Farrell and Clark, 1976; Milne and Mitrovica, 1998). Since not all load information for 2015 and 2016 is available yet, we will limit the time series of ALT-TG up to 2015. The GNSS trends are pre-computed and therefore we linearly extrapolate the fingerprint data, is necessary, to 2015 and 2016 by taking the difference between years 2013 and 2014.

3 Results

This section first addresses the trends obtained from GNSS stations. The averaging methods are discussed and the NGL trends are compared to those of ULR. Then the results of the correlation-weighted ALT-TG trends are discussed. These are compared to those from Wöppelmann and Marcos (2016). After that, the GNSS and ALT-TG trends are compared and optimal settings are discussed. For the comparison we take into account that both trends are not computed from time series covering the same period by correcting for non-linear VLM trends estimated from fingerprints.

3.1 Direct GNSS trends

For 570 TGs at least one GNSS station is found within a 50 km radius with an uncertainty on the trend that is below 1 mm yr^{-1} . The VLM for these TGs is shown in Fig. 2 using the median of the surrounding GNSS stations in case there are multiple trends available. The signature of GIA dominates the signal on large scales, which is primarily visible in Scandinavia and Canada.

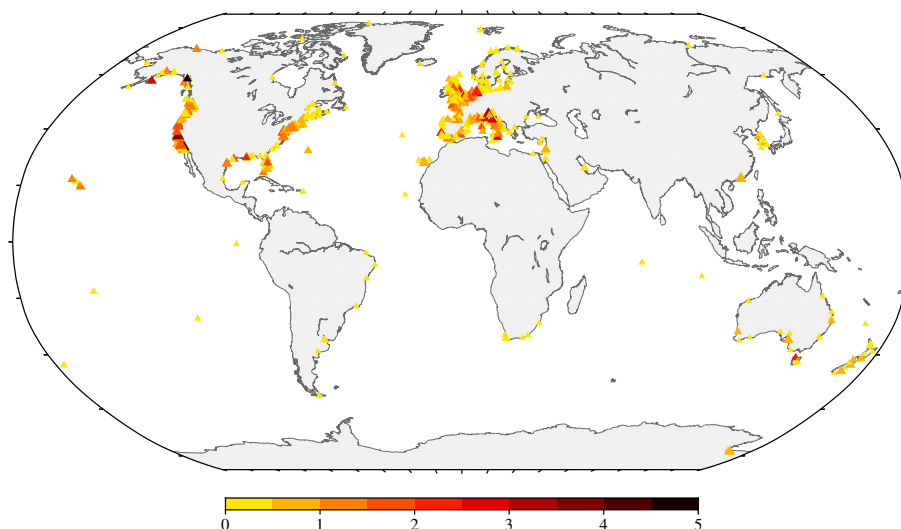


Figure 3. Spread (mm/yr) in VLM at TGs using eight different approaches. The size of the symbols indicates the number of GNSS trends available (with a maximum of ten).

Table 3. Statistics of trend differences between NGL and ULR at 70 stations for various weighting techniques.

	RMS	Mean	Median
Approach	mm yr ⁻¹	mm yr ⁻¹	mm yr ⁻¹
1	1.11	0.07	0.05
2	1.05	0.12	0.03
3	1.36	0.02	0.02
4	1.21	0.00	0.03
5	1.29	0.32	0.20
6	1.15	0.24	0.17
7	1.11	0.08	0.02
8	1.23	0.01	0.05

In Alaska there might be a significant contribution of present-day ice mass loss. If GIA is removed the VLM signals typically range between -3 and 3 mm yr⁻¹ (Wöppelmann and Marcos, 2016), with a few exceptions.

Even though the large-scale GIA process appears to be captured properly, regional VLM has a large effect on the GNSS trends. In Fig. 3 the differences between the lowest and highest VLM estimate from the eight methods discussed in Sect. 2.1.2 are shown. The extreme values primarily resulted from the 'mean', 'median' and 'inverse distance' weighting methods (not shown). The figure shows that the spread is generally higher, where more GNSS trends are available. In particular the seismically active zones like the US West Coast show a larger spread. The spread between solutions, when considering all TGs with at least two GNSS trends, has a mean of 0.92 mm yr⁻¹ and a median of 0.71 mm yr⁻¹. In case at least three available



Table 4. Number of TGs at which trends are estimated from differenced ALT-TG time series. The '-1.0' indicates no correlation threshold is set.

Threshold	Number of TGs
-1.0	663
0.0	660
0.1	658
0.2	655
0.3	638
0.4	602
0.5	549
0.6	470
0.7	344

GNSS trends are considered, the differences rise to 1.09 mm yr^{-1} and 0.85 mm yr^{-1} , respectively. Since we only considered GNSS trends with a maximum standard deviation of 1 mm yr^{-1} , this implies that a significant contribution of kilometer-scale VLM variations is present along the West Coast of the US, where the difference between methods is often larger than 1 mm yr^{-1} . Note that the spread between individual GNSS trends is on average even larger than the spread between methods.

5 *Santamaría-Gómez et al. (2017)* estimated the global numbers for the impact of spatial variations in VLM at 30 km and 100 km separation to be 0.2 mm yr^{-1} and 0.5 mm yr^{-1} . However, at several coastal locations, especially in Europe and North America this appears to be an underestimation. The differences between methods is often comparable in size as the VLM signal, especially after the GIA is removed.

Wöppelmann and Marcos (2016) show that a comparison between their ALT-TG trends and their GNSS trends yields an
10 RMS of 1.47 mm yr^{-1} . They use visual inspection to remove tide gauges where clear non-linear effects or discontinuities were present. In Table 3 a comparison is made between the eight different weighting methods and the GNSS trends of *Wöppelmann and Marcos (2016)* that were used in the aforementioned comparison with ALT-TG trends at 70 locations. The values show that a substantial fraction of the RMS between direct and differenced trends can already be explained by different GNSS averaging and processing methods. Using the closest station (approach 3) an RMS of 1.36 mm yr^{-1} , which is comparable in magnitude
15 to the RMS between GNSS and ALT-TG trends found by *Wöppelmann and Marcos (2016)*. The best comparison is found with the median (approach 2), even though the RMS of differences is still above 1 mm yr^{-1} .

3.2 Differenced ALT-TG trends

Using correlation thresholds, we try to minimize the residual ocean signal in ALT-TG time series. Additionally, it will filter problematic stations, where no correlation between TG and altimetry observations is found. A higher threshold reduces there-
20 fore the number of ALT-TG trends. Table 4 shows the reduction of the differenced VLM trends, when the correlation threshold increases. After a correlation threshold of 0.4, the number of observations drops substantially. At a threshold of 0.7, the number

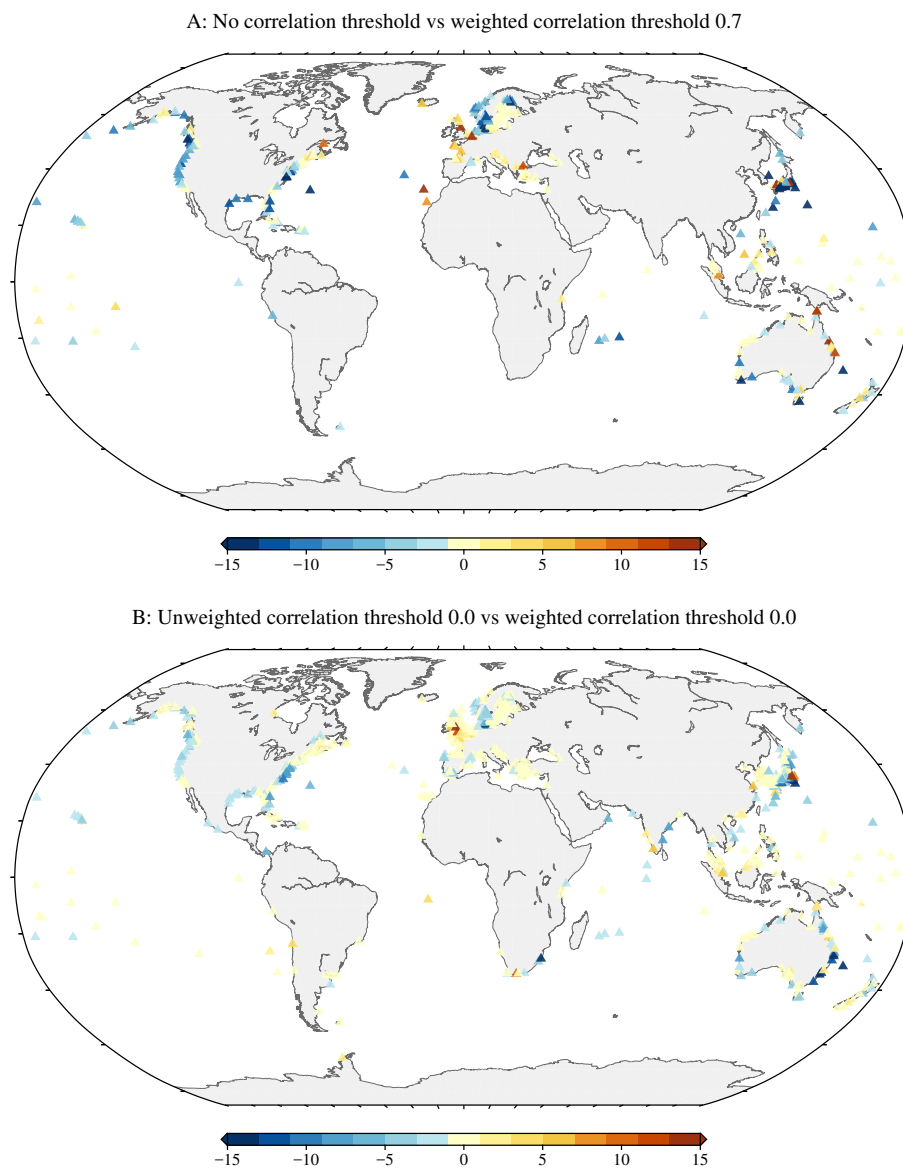


Figure 4. Reduction in standard deviation (mm) of the differenced time series using correlation thresholds and weighting. Note that a correlation threshold of 0.0 indicates positive correlations only.

of TGs for which a trend is computed, is only half of that without a threshold. The remaining trends are generally more reliable, because of two reasons: VLM time series that exhibit relatively large residual ocean signals are removed; and secondly, TG time series that contain large jumps due to unidentified reasons (e.g. earthquakes or equipment changes) are removed.

In order to show that the method decreases the oceanic signal, we compare the standard deviation reduction by using correlation thresholds and weighting (Fig. 4). The plot in the top panel shows the comparison between the standard deviation of the

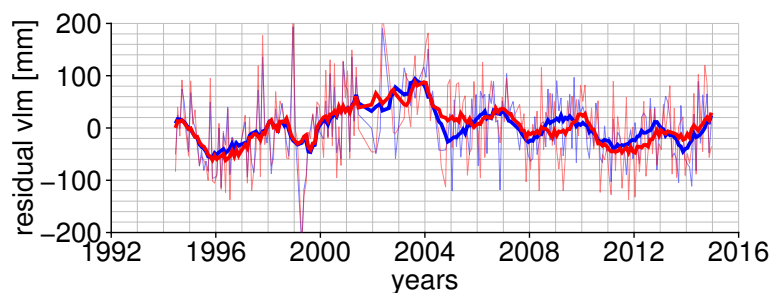


Figure 5. Low-pass filtered time series of ALT-TG differenced VLM at the Llandudno (UK) TG. In blue: with a threshold of 0.0 for the correlation, but without correlation weighting. In red: with a threshold of 0.0 for the correlation and with correlation weighting. In the background the time series without a low-pass filter applied.

differenced time series using no correlation threshold and the time series using a threshold of 0.7 together with a correlation weighting. The mean reduction in standard deviation is 3.9 mm, whereas the mean standard deviation is 37 mm. The change in standard deviations at several locations are coherent, which is expected because the sea level fluctuations along continental slopes are coherent (*Hughes and Meridith, 2006*). Substantial reductions in standard deviation are apparent at both North American coasts, in Japan and in Northern Europe. *Vinogradov and Ponte (2011)* had already observed large discrepancies in interannual ocean signals between TGs and altimetry in North America and in Japan. It suggests that our technique is capable to reduce these ocean signals. The Winter Harbour (Canada) VLM time series (Fig. 1) shows a typical example in which especially the correlated noise is reduced. However, there are several locations where the standard deviation increases substantially. Most of them are sporadic, but in a few locations, like in the UK and France there is coherent increase. Though reduced in magnitude, similar, patterns are observed for the not-weighted against weighted VLM time series with a correlation threshold of 0.0 (bottom of Fig. 4), i.e. when only positively correlated altimetry time series are taken into account. Instead of 344 VLM trends, as for the comparison discussed above, 660 trends are compared. The mean reduction of the standard deviation is 1.4 mm, whereas the mean standard deviation is 38 mm. Remarkable is the strong reduction of the standard deviation at the southeast side of Australia. In the UK and France an increase in standard deviation is present again. In most cases an increase in white noise, likely due to the decreased effective number of altimetry measurements, is responsible for the higher standard deviation, as demonstrated in Fig. 5 for a VLM time series at Llandudno, UK. In most cases of an increasing standard deviation, the correlated ocean signals are still reduced or remain approximately equal.

Fig. 6 shows the VLM trends estimated from the ALT-TG time series using no correlation threshold and a threshold of 0.7. A comparison of Fig. 2 and Fig. 6 reveals that especially the Indian Ocean and the southern Pacific Ocean are sampled better using ALT-TG instead of GNSS trends. If the correlation threshold is set to 0.7, the number of trends decreases, which has particularly an impact on the number of trends in South America and Africa. Hence, for regional reconstructions, a careful choice should be made for the correlation threshold.

Compared to the GNSS trends, the neighbouring ALT-TG trends show more variation, which is especially true for the UK and Japan. It is difficult to say whether this is a true VLM signal, but it is important to note that many GNSS stations

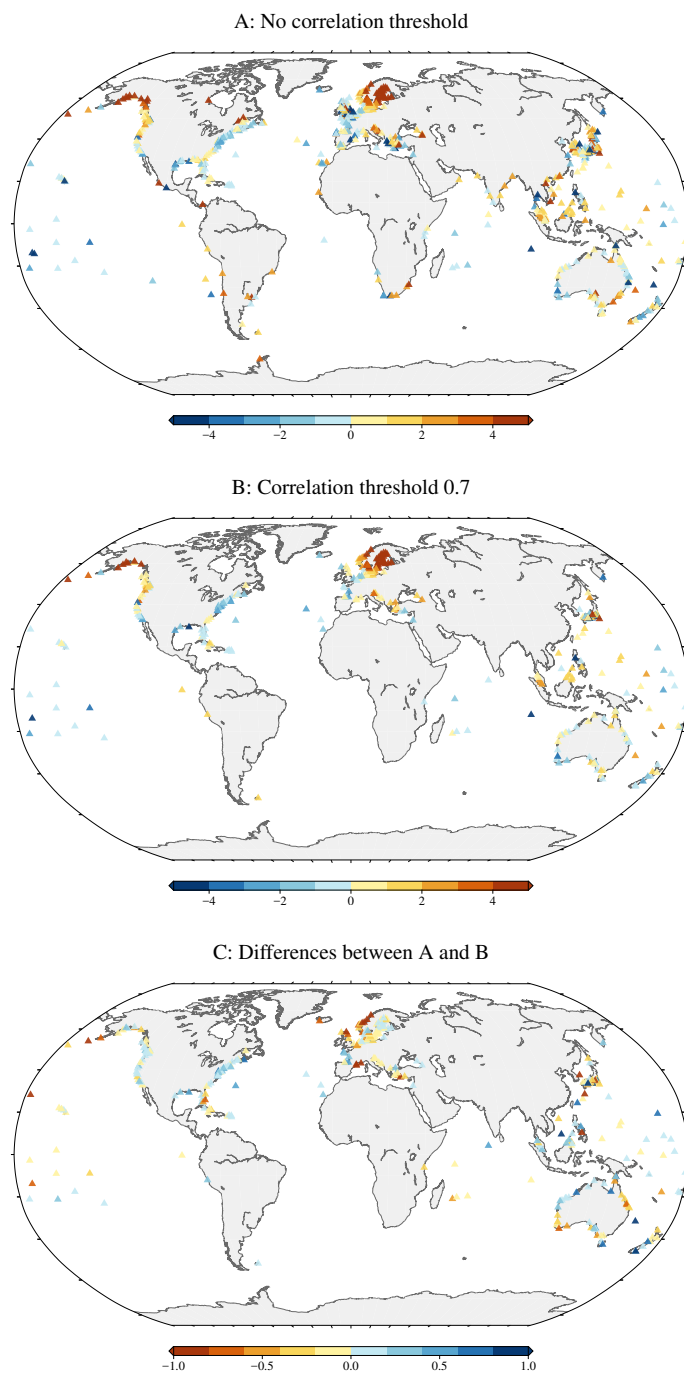


Figure 6. ALT-TG trends (mm yr^{-1}) estimated using no threshold (A), with a correlation threshold and correlation weighting (B) and the difference between them (C).

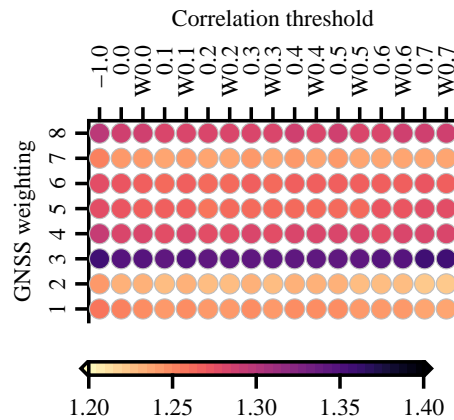


Figure 7. RMS (mm/yr) of differences between direct and indirect inferred VLM trends. The 'W' indicates weighting by correlation. The '-1.0' indicates no correlation threshold is set. The numbers of the y-axis refer to the weighting methods for GNSS trends as described in Sect. 2.1.2.

are placed on bedrock, which exhibits more stable trends than the coastal locations of tide gauges. Secondly, the GNSS trends with an error larger than 1 mm yr^{-1} are removed, which reduces the variability. However, the larger trend variability can also be induced by remaining ocean signal in the VLM time series. In the Fig. 6B, showing the 0.7 threshold trends, the number of trends is reduced due to the correlation threshold. It removes most tide gauges in the highly variable regions mentioned before and the neighbouring differences are therefore less erratic.

The results of applying correlation weighting and thresholding are shown Fig. 6C. Two spots of coherent changes in the trends can be clearly identified: in Norway the trends increased by approximately 1 mm yr^{-1} , while in the East Coast of the United states the opposite happens. These spots exhibit longshore coherent sea level signals that are not found in the open ocean (Calafat *et al.*, 2013; Andres *et al.*, 2013). Note that both locations also exhibit a strong reduction in standard deviation (Fig. 4). Coherent changes are also present around Denmark. Other regions, where substantial reductions in the standard deviation are found, do not experience coherent changes in trends.

3.3 GNSS vs ALT-TG trends

In this section the VLM trends from GNSS using the eight weighting solutions as described in Sect. 2.1.2 are compared with the differenced ALT-TG VLM trends using various correlation thresholds. Based on the intercomparison we determine the best solution for the GNSS weighting and the correlation thresholds for altimetry. Additionally, a comparison is made with Wöppelmann and Marcos (2016). We also investigate the effect of present-day mass redistribution on the difference in trends due to varying time spans of the direct and the differenced method.

Fig. 7 shows the RMS of trends differences between various GNSS weighting methods and correlation thresholds for ALT-TG. The RMS of trend differences is computed at 155 TG stations for which all solutions are available. The colors exhibit small differences horizontally and large differences vertically, indicating that the GNSS weighting method is more important



Table 5. Statistics of the differences between the GNSS trends using median weighting and the ALT-TG trends for various correlations thresholds. The 'W' indicates that the altimetry time series are weighted by the correlation. The row 'W&M' shows the comparison with *Wöppelmann and Marcos* (2016) trends. The column 'NoT' indicates the number of trends. On the left side of the table all stations are taken into account, on the right side only stations are taken into account for which a solution exist for all correlations thresholds (and including those from W&M).

Correlation	All				Same			
	RMS	Mean	Median	NoT	RMS	Mean	Median	NoT
	mm yr ⁻¹	mm yr ⁻¹	mm yr ⁻¹		mm yr ⁻¹	mm yr ⁻¹	mm yr ⁻¹	
-1.0	2.141	-0.241	-0.107	294	1.234	-0.167	-0.099	137
0.0	2.108	-0.248	-0.101	294	1.226	-0.175	-0.068	137
0.0W	2.103	-0.250	-0.036	294	1.219	-0.172	-0.056	137
0.1	2.113	-0.258	-0.096	293	1.219	-0.174	-0.074	137
0.1W	2.108	-0.260	-0.043	292	1.218	-0.170	-0.045	137
0.2	2.082	-0.233	-0.073	292	1.217	-0.163	-0.074	137
0.2W	2.080	-0.234	-0.015	292	1.216	-0.168	-0.042	137
0.3	1.986	-0.152	0.047	283	1.221	-0.157	-0.066	137
0.3W	1.991	-0.157	0.056	283	1.217	-0.165	-0.044	137
0.4	1.695	-0.106	0.065	264	1.223	-0.152	-0.050	137
0.4W	1.696	-0.112	0.071	264	1.218	-0.158	-0.041	137
0.5	1.554	-0.086	0.044	239	1.220	-0.153	-0.058	137
0.5W	1.552	-0.087	0.056	239	1.217	-0.155	-0.067	137
0.6	1.417	-0.093	-0.065	204	1.209	-0.155	-0.087	137
0.6W	1.416	-0.093	-0.083	204	1.208	-0.156	-0.094	137
0.7	1.220	-0.142	-0.123	155	1.206	-0.140	-0.060	137
0.7W	1.220	-0.144	-0.124	155	1.206	-0.142	-0.074	137
W&M	1.658	-0.177	-0.050	211	1.328	-0.101	0.020	137

in reducing the RMS. The difference between the method with the lowest RMS of differences, which is obtained by taking the median of the GNSS trends (2), and the method with the highest RMS, which uses the closest GNSS station (3), is approximately 0.14 mm yr⁻¹. *Hamlington et al.* (2016) computed VLM trends at TG locations by using a complex filtering procedure that also implicitly takes into account the median of the GNSS trends. Next to taking the median of the GNSS trends, taking the mean (1) within the 50 km radius and using variance weighting (7) also yield substantially lower RMS differences than the other five methods. However, the median method performs slightly better. Besides, it inherently takes into account the standard deviation of the GNSS trends (which is not done by taking the mean) and it filters the spatial variations in VLM (which is not done by variance weighting).

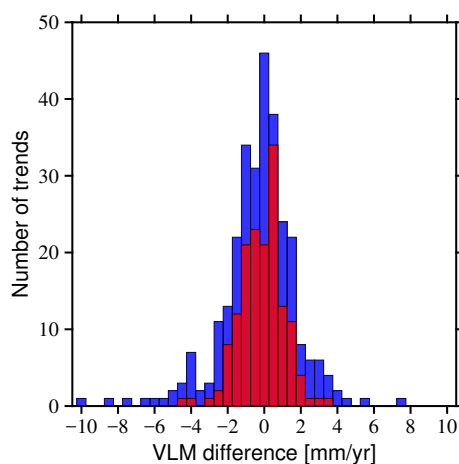


Figure 8. Histogram of GNSS and ALT-TG trend differences. In blue the results without any correlation threshold and in red with a correlation threshold of 0.7 and correlation weighting.

In Table 5 we analyze the results for different correlation thresholds in more detail by comparing them to the GNSS trends based on the median method. On the left side of the table the RMS, mean and median are shown for all VLM estimates available for each correlation threshold. Setting no correlation thresholds yields 294 trends for comparison, while setting a threshold at 0.7 leaves only 155. While the number of trends decreases, the RMS decreases as well, indicating that the correlation thresholds can serve as a selection procedure, which filters out outliers. This is confirmed by Fig. 8, in which we see the decrease of the number of available trends, but also the removal of the outliers. If the threshold is set to 0.7 only three discrepancies in trends of larger than 3 mm yr⁻¹ are found. Note that the reduction in RMS is not only caused by the removal of problematic ALT-TG time series. Large earthquakes for example might induce jumps or non-linear behaviour in both the TG and GNSS time series, so the larger spread in Fig. 8 for no correlation threshold may be partly attributed to problematic GNSS trends. In the last row the *Wöppelmann and Marcos (2016)* trends are compared with our GNSS trends. It has a similar RMS with the 0.4-0.5 correlation threshold trends, but it is computed with a substantially smaller number of trends.

On the right side of the table, we only included TGs for which all solutions are available, which reduces the number from 155 to 137, because W&M trends are also considered for comparison. The RMS of differences for 155 stations is only slightly larger as will be shown below in Table 6. Note that the RMS of the residuals using ALT-TG from W&M, is already 0.14 mm yr⁻¹ lower than those in the study of *Wöppelmann and Marcos (2016)* and about 0.4 mm yr⁻¹ less than in *Pfeffer and Allemand (2016)*, who incorporated only 109 and 113 stations, respectively. This is a consequence of the combined use of the NGL trends with median weighting and the selection based on correlation. Our altimetry solutions further decrease the RMS by another 0.1 mm yr⁻¹ compared to W&M, even when no threshold on the correlation is set. In the study of *Wöppelmann and Marcos (2016)*, the along-track altimetry ALT-TG trends performed worse than the AVISO results. The reason for this discrepancy could be the latitudinal intermission bias, or the small radius around the TG used in that study for including altimetry measurements.

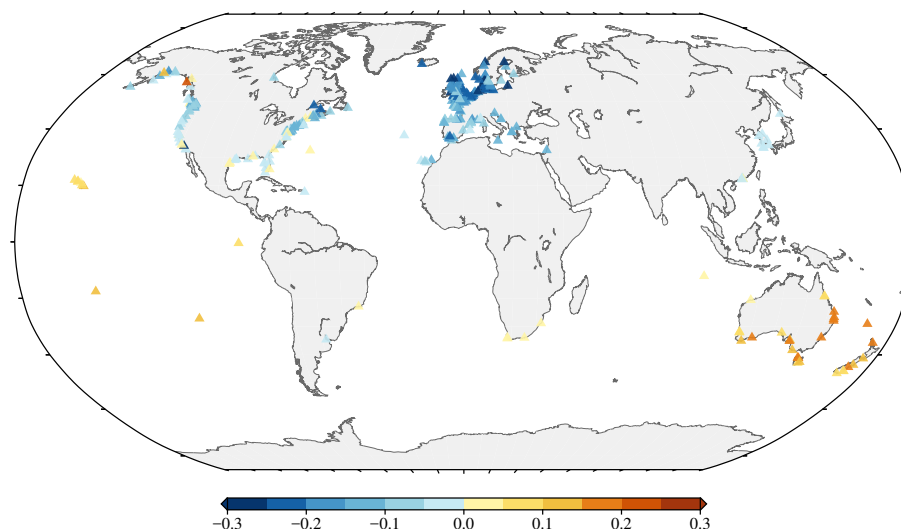


Figure 9. Trend differences (mm yr^{-1}) between the GNSS and ALT-TG time spans induced by non-linear VLM due to present-day mass redistribution.

Increasing the correlation threshold only slightly reduces the RMS between GNSS and ALT-TG trends and the additional weighting has a neglectable effect on the RMS. As mentioned before, the threshold increase and weighting generally reduced the standard deviation (Fig. 4) of the ALT-TG time series and Fig. 6 showed coherent changes in trend. Additionally, the NGL and ULR trends showed an RMS of differences and the weighting methods spreads of more than a millimeter. We argue that the absence of a clear improvement or a change in RMS due to correlation thresholds is a result of the relatively large noise in the GNSS trends. The histogram in Fig. 8 shows that for 155 stations, only three discrepancies are larger than 3 mm yr^{-1} . These TGs (which are located at Galveston (US), Eureka (US) and the Cocos Islands (Australia)) are all inspected and we find that the neighbouring GNSS stations are located at the other side of lagoons or on different islands. The GNSS is therefore the likely cause for the largest discrepancies and not the ALT-TG trend.

The third column of Table 5 shows that the mean is in all cases negative, i.e. the GNSS trends are larger than those of ALT-TG. Trends obtained with correlations -1.0, 0.0, 0.1 and 0.2 are barely statistically different from zero based on a 95% confidence level, while the others are not. The 95 % confidence level is taken as two times the standard deviation of the mean of the residual trends ($\frac{\sigma_n}{\sqrt{N}}$, where N is the number of trends and σ_n the standard deviation of the residual trends). In the right 'mean' column for the 137 stations, the means are statistically insignificantly different from zero at the 95%-confidence level, whereas at a 90%-confidence level several are not. The medians in both columns are closer to zero and deviate up to 0.2 mm yr^{-1} from the mean, which indicates a slightly skewed distribution.

There is a non-linear VLM signal due to present-day mass loss in both GNSS and ALT-TG trends and since they cover different time spans this causes small systematic differences between trends. Due to the inhomogeneous distribution of the TGs and the spatial signal of non-linear VLM, this does not only affect the mean, but also the skewness of the distribution. In



Table 6. Statistics of trend differences with GPS for various solutions after applying a correction for non-linear VLM.

Correlation	NoT: 155			NoT: 137		
	RMS mm yr ⁻¹	Mean mm yr ⁻¹	Median mm yr ⁻¹	RMS mm yr ⁻¹	Mean mm yr ⁻¹	Median mm yr ⁻¹
-1.0	1.231	-0.102	-0.039	1.223	-0.100	0.030
0.0	1.225	-0.109	-0.027	1.215	-0.108	0.031
0.0	1.223	-0.106	0.016	1.209	-0.105	0.048
0.1	1.220	-0.107	-0.014	1.208	-0.107	0.034
0.1	1.222	-0.104	0.003	1.208	-0.104	0.072
0.2	1.220	-0.099	0.016	1.207	-0.096	0.027
0.2	1.221	-0.101	-0.001	1.206	-0.101	0.059
0.3	1.223	-0.091	0.011	1.211	-0.090	0.018
0.3	1.221	-0.098	-0.001	1.207	-0.098	0.036
0.4	1.226	-0.087	0.011	1.214	-0.085	0.021
0.4	1.223	-0.092	0.008	1.209	-0.091	0.037
0.5	1.225	-0.088	0.020	1.212	-0.086	0.042
0.5	1.222	-0.090	0.027	1.208	-0.088	0.045
0.6	1.222	-0.087	-0.007	1.202	-0.088	0.018
0.6	1.222	-0.087	-0.006	1.201	-0.089	0.028
0.7	1.220	-0.071	0.021	1.202	-0.073	0.037
0.7	1.219	-0.074	0.012	1.201	-0.075	0.036

Fig. 9 the trend difference between the GNSS and ALT-TG methods are visualized for all 294 stations. Most of the negative differences in trends are observed in Europe and parts of North-America, while positive differences in trends are observed in Australia. In Europe there is an uplift due to present-day mass loss, which increases over the last few years. Since the GNSS time series are generally shorter, they measure a larger uplift signal. By subtracting the present-day VLM that GNSS observes from altimetry observations, we obtain negative signals in Europe.

We applied a correction for the effect of present-day mass loss to the trends for the 155 stations for which a trend is found with all methods in Table 6. Similarly, this is done for the 137 stations, so that the results are comparable with Table 5. There is no significant reduction in RMS. The maximal deviation of the median from zero is 0.06 mm yr⁻¹ for the 155 stations and maximally 0.07 mm yr⁻¹ for the 137 stations, which is a reduction with respect to the values listed in Table 5. The mean is also reduced to approximately -0.1 mm yr⁻¹, which is statistically equal to zero. This result is at the level of the noise in the determination of the ITRF origin (*Santamaría-Gómez et al., 2017*) and it is smaller than the 0.4 mm yr⁻¹ to which global mean sea level trends from altimetry are guaranteed (*Mitchum, 2000*). Unless it is proven that the altimeters are more stable and the uncertainties in the ITRF origin are reduced, a mean of trend differences closer to zero cannot be expected.



4 Conclusions

We presented new ways to estimate VLM at TGs from GNSS observations and differenced ALT-TG time series. A comparison is made between eight different weighting methods to obtain VLM at the TG from NGL GNSS trends. The spread of the trends between the weighting methods is at the same level as the standard deviations of the GNSS trends, with a mean of 0.92 mm yr⁻¹ and a median of 0.71 mm yr⁻¹. A comparison with the estimates of ULR5 (Wöppelmann and Marcos, 2016) at 70 stations yielded an RMS of at least 1.05 mm yr⁻¹. A comparison with ALT-TG showed that using the median of all neighbouring GNSS provided the best results.

For the ALT-TG trends we used along-track observations from the Jason series of altimeters. At every 6 km along-track observations were stacked, to create time series. The time series were low-pass filtered with a moving-average filter of one year and correlated with low-pass filtered TG time series. An average or weighted monthly time series for altimetry was created taking only into account the time series corresponding to correlations above a threshold. The TG time series were subtracted from the average of monthly low-pass filtered altimetry time series to create a ALT-TG time series. Using the Hector software between 344 and 663 trends were computed from the ALT-TG time series, depending on the correlation threshold set.

The standard deviation of the ALT-TG time series was reduced on average by approximately 10 % when a correlation threshold of 0.7 was used. Spatially coherent differences in trends between various thresholds are observed at the east coast of the US and in Norway. We argue that residual interannual ocean variability in ALT-TG time series can locally induce VLM trend biases, especially when time series are short. For 155 stations globally distributed, increasing the correlation threshold does not significantly affect the RMS of differences between GNSS and ALT-TG trends. However, the correlation threshold also works as a selection procedure. When considering 294 VLM estimates from GNSS and ALT-TG at the same TGs for comparison, with no threshold yielded an RMS of differences of 2.14 mm yr⁻¹, whereas an RMS of 1.22 mm yr⁻¹ was reached using 155 stations and a threshold of 0.7. This is a substantial improvement with respect to the 1.47 mm yr⁻¹ RMS of Wöppelmann and Marcos (2016) at 109 TGs, the best result so far. Note that increasing the threshold considerably reduces the number of time series in the southern hemisphere and therefore other thresholds might be better depending on the purpose.

The comparison with tide gauges also reveals that the trends from ALT-TG are biased low (similar to Wöppelmann and Marcos (2016)), even though this is barely significant. Using mass redistribution fingerprints, a correction is applied for trend differences caused by non-linear behaviour of present-day mass changes. The RMS of differences is barely affected, but the mean of differences is changed from about -0.2 to -0.1 mm yr⁻¹, which is now statistically insignificant.

The trends in this publication (median GNSS and ALT-TG for all correlations) will be made publicly available. When no correlation threshold is used this implies that 663 ALT-TG and 570 GNSS trends are available at 939 different TGs. Setting the correlation threshold to 0.7, the number of trends at different TGs decreases to 759. Depending on the application, the value of the threshold can be varied to find an optimum between the reliability and the number of trends. If both GNSS and ALT-TG trends are available, we recommend to use GNSS trends, because of correlated residual ocean signals between various ALT-TG time series. However, if a large discrepancy (> 3 mm yr⁻¹) is found between the GNSS and ALT-TG trends, we recommend to use the ALT-TG trend, because the culprit is likely local VLM differences between the TG and the GNSS stations. The GNSS -



ALT-TG histogram for no correlation threshold reveals large discrepancies between the two methods up to 10 mm yr^{-1} . While the problem with ALT-TG trends are mostly resolved by setting a higher threshold, the GNSS trends might still require some inspection before they are used in sea level studies.

Acknowledgements. This study is funded by the Netherlands Organisation for Scientific Research (NWO) through VIDI grant 864.12.012

5 (Multi-Scale Sea Level (MuSSeL)).

The MIDAS GNSS trends are obtained from the Nevada Geodetic Laboratory (NGL).

<http://geodesy.unr.edu/>

The altimetry data are obtained from the Radar Altimetry Database System (RADS).

<http://rads.tudelft.nl/rads/rads.shtml>

10 Permanent Service for Mean Sea Level (PSMSL), 2017, "Tide Gauge Data", Retrieved 1 November 2016.

<http://www.psmsl.org/data/obtaining/>

We would like to thank Marta Marcos and Guy Wöppelmann for sharing their trend estimates.



References

- Ablain, M., Cazenave, A., Larnicol, G., Balmaseda, M., Cipollini, P., Faugère, Y., ... & Benveniste, J. (2015). Improved sea level record over the satellite altimetry era (1993-2010) from the Climate Change Initiative Project. *Ocean Science*, 11, 67-82.
- Andres, M., Gawarkiewicz, G. G., & Toole, J. M. (2013). Interannual sea level variability in the western North Atlantic: Regional forcing and remote response. *Geophysical Research Letters*, 40(22), 5915-5919.
- 5 Blewitt, G., Kreemer, C., Hammond, W. C., & Gazeaux, J. (2016). MIDAS robust trend estimator for accurate GPS station velocities without step detection. *Journal of Geophysical Research: Solid Earth*, 121, 2054-2068, doi:10.1002/2015JB012552.
- Bos, M. S., Fernandes, R. M. S., Williams, S. D. P., & Bastos, L. (2013). Fast error analysis of continuous GNSS observations with missing data. *Journal of Geodesy*, 87(4), 351-360.
- 10 Bos, M. S., Williams, S. D. P., Araújo, I. B., & Bastos, L. (2013). The effect of temporal correlated noise on the sea level rate and acceleration uncertainty. *Geophysical Journal International*, 196(3), 1423-1430.
- Bouin, M. N., & Wöppelmann, G. (2010). Land motion estimates from GPS at tide gauges: a geophysical evaluation. *Geophysical Journal International*, 180(1), 193-209.
- Calafat, F. M., Chambers, D. P., & Tsimplis, M. N. (2013). Inter-annual to decadal sea-level variability in the coastal zones of the Norwegian and Siberian Seas: The role of atmospheric forcing. *Journal of Geophysical Research: Oceans*, 118(3), 1287-1301.
- 15 Carrère, L., & Lyard, F. (2003). Modelling the barotropic response of the global ocean to atmospheric wind and pressure forcing - comparisons with observations. *Geophysical Research Letters*, 30(6), 1275, 2003.
- Cazenave, A., Dominh, K., Ponchaut, F., Soudarin, L., Cretaux, J. F., & Le Provost, C. (1999). Sea level changes from Topex-Poseidon altimetry and tide gauges, and vertical crustal motions from DORIS. *Geophysical Research Letters*, 26(14), 2077-2080.
- 20 Desai, S., Wahr, J., & Beckley, B. (2015). Revisiting the pole tide for and from satellite altimetry. *Journal of Geodesy*, 89(12), 1233-1243.
- Ducet, N., Le Traon, P. Y., & Reverdin, G. (2000). Global high-resolution mapping of ocean circulation from TOPEX/Poseidon and ERS-1 and -2. *Journal of Geophysical Research: Oceans*, 105(C8), 19477-19498.
- Farrell, W. E., & Clark, J. A. (1976). On postglacial sea level. *Geophysical Journal International*, 46(3), 647-667.
- Frederikse, T., Riva, R., Kleinherenbrink, M., Wada, Y., Broeke, M., & Marzeion, B. (2016). Closing the sea level budget on a regional scale: Trends and variability on the Northwestern European continental shelf. *Geophysical Research Letters*, 43(20).
- 25 Gazeaux, J., Williams, S., King, M., Bos, M., Dach, R., Deo, M., Moore, A. W., Ostini, L., Petrie E., Roggero, M., Teferle, F. N., Olivares, G., & Webb, F.H. (2013). Detecting offsets in GPS time series: First results from the detection of offsets in GPS experiment. *Journal of Geophysical Research: Solid Earth*, 118(5), 2397-2407.
- Hamlington, B. D., Thompson, P., Hammond, W. C., Blewitt, G., & Ray, R. D. (2016). Assessing the impact of vertical land motion on twentieth century global mean sea level estimates. *Journal of Geophysical Research: Oceans*, 121(7), 4980-4993.
- 30 Hughes, C.W., & Meredith, M.P. (2006). Coherent sea-level fluctuations along the global continental slope. *Phil. Trans. R. Soc.*, 364, 885-901.
- Holgate, S. J., Matthews, A., Woodworth, P. L., Rickards, L. J., Tamsiea, M. E., Bradshaw, E., Foden, P. R., Gordon, K. M., Jevrejeva, S., & Pugh, J. (2012). New data systems and products at the permanent service for mean sea level. *Journal of Coastal Research*, 29(3), 493-504.
- Masters, D., Nerem, R. S., Choe, C., Leuliette, E., Beckley, B., White, N., & Ablain, M. (2012). Comparison of global mean sea level time series from TOPEX/Poseidon, Jason-1, and Jason-2. *Marine Geodesy*, 35(sup1), 20-41.
- 35 Milne, G. A., & Mitrovica, J. X. (1998). Postglacial sea-level change on a rotating Earth. *Geophysical Journal International*, 133(1), 1-19.



- Mitchum, G. T. (1998). Monitoring the stability of satellite altimeters with tide gauges. *Journal of Atmospheric and Oceanic Technology*, 15(3), 721-730.
- Mitchum, G. T. (2000). An improved calibration of satellite altimetric heights using tide gauge sea levels with adjustment for land motion. *Marine Geodesy*, 23(3), 145-166.
- 5 Nerem, R. S., & Mitchum, G. T. (2002). Estimates of vertical crustal motion derived from differences of TOPEX/POSEIDON and tide gauge sea level measurements. *Geophysical Research Letters*, 29(19).
- Ostanciaux, É., Husson, L., Choblet, G., Robin, C., & Pedoja, K. (2012). Present-day trends of vertical ground motion along the coast lines. *Earth-Science Reviews*, 110(1), 74-92.
- Petit, G., & Luzum, B. (2010). IERS conventions (2010) (No. IERS-TN-36). BUREAU INTERNATIONAL DES POIDS ET MESURES
- 10 SEVRES (FRANCE).
- Pfeffer, J., & Allemand, P. (2016). The key role of vertical land motions in coastal sea level variations: a global synthesis of multisatellite altimetry, tide gauge data and GPS measurements. *Earth and Planetary Science Letters*, 439, 39-47.
- Pujol, M. I., Faugère, Y., Taburet, G., Dupuy, S., Pelloquin, C., Ablain, M., & Picot, N. (2016). DUACS DT2014: the new multi-mission altimeter data set reprocessed over 20 years. *Ocean Science*, 12(5).
- 15 Ray, R. D., Beckley, B. D., & Lemoine, F. G. (2010). Vertical crustal motion derived from satellite altimetry and tide gauges, and comparisons with DORIS measurements. *Advances in Space Research*, 45(12), 1510-1522.
- Riva, R. E., Frederikse, T., King, M. A., Marzeion, B., & van den Broeke, M. R. (2017). Brief communication: The global signature of post-1900 land ice wastage on vertical land motion. *The Cryosphere*, 11(3), 1327.
- Santamaría-Gómez, A., Gravelle, M., Collilieux, X., Guichard, M., Míguez, B. M., Tiphaneau, P., & Wöppelmann, G. (2012). Mitigating the
- 20 effects of vertical land motion in tide gauge records using a state-of-the-art GPS velocity field. *Global and Planetary Change*, 98, 6-17.
- Santamaría-Gómez, A., Gravelle, M., Dangendorf, S., Marcos, M., Spada, G., & Wöppelmann, G. (2017). Uncertainty of the 20th century sea-level rise due to vertical land motion errors. *Earth and Planetary Science Letters*, 473, 24-32.
- Santamaría-Gómez, A., Gravelle, M., & Wöppelmann, G. (2014). Long-term vertical land motion from double-differenced tide gauge and satellite altimetry data. *Journal of Geodesy*, 88(3), 207-222.
- 25 Scharroo, R., Leuliette, E. W., Lillibridge, J. L., Byrne, D., Naeije, M. C., & Mitchum, G. T. (2012). RADS: Consistent multi-mission products. In *Proceedings of Symposium on 20 Years of Progress in Radar Altimetry (Vol. 20)*.
- Vinogradov, S. V., & Ponte, R. M. (2011). Low-frequency variability in coastal sea level from tide gauges and altimetry. *Journal of Geophysical Research: Oceans*, 116(C7).
- Watson, C. S., White, N. J., Church, J. A., King, M. A., Burgette, R. J., & Legresy, B. (2015). Unabated global mean sea-level rise over the
- 30 satellite altimeter era. *Nature Climate Change*, 5(6), 565-568.
- Williams, S. D. P. (2008). CATS: GPS coordinate time series analysis software. *GPS Solutions*, 12(2), 147-153, doi:10.1007/s10291-007-0086-4.
- Wöppelmann, G., Míguez, B. M., Bouin, M. N., & Altamimi, Z. (2007). Geocentric sea-level trend estimates from GPS analyses at relevant tide gauges world-wide. *Global and Planetary Change*, 57(3), 396-406.
- 35 Wöppelmann, G., Marcos, M., Santamaría-Gómez, A., Martín-Míguez, B., Bouin, M. N., & Gravelle, M. (2014). Evidence for a differential sea level rise between hemispheres over the twentieth century. *Geophysical Research Letters*, 41(5), 1639-1643.
- Wöppelmann, G., & Marcos, M. (2016). Vertical land motion as a key to understanding sea level change and variability. *Reviews of Geophysics*, 54(1), 64-92.